Journal of Nepal Geological Society, 2001, Vol. 25 (Sp. Issue), pp. 99–109

Magnetostratigraphic evidence for the occurrence of pre-Brunhes (>780 kyr) sediments in the northwestern part of the Kathmandu Valley, Nepal

Pitambar Gautam[1], Azumi Hosoi[2], Tetsuya Sakai[3] and Kazunori Arita[2]

[1]*Central Department of Geology, Tribhuvan University, Kirtipur, Kathmandu, Nepal*
(Corresponding author, e-mail: pgautam2000@yahoo.com)

[2]*Division of Earth and Planetary Sciences, Graduate School of Science, Hokkaido University, Sapporo 060-0810, Japan*

[3]*Department of Geology and Mineralogy, Division of Earth and Planetary Sciences, Graduate School of Science, Kyoto University, Kyoto 606-8502, Japan*

ABSTRACT

Fine-grained silt/clay sediments constituting several sections of the fluvio-lacustrine sediments distributed in the central and northwestern parts of the Kathmandu Valley have been studied for the magnetic polarity stratigraphy. These sediments carry a stable primary remanence, residing in hematite and/or magnetite, which is isolated after alternating field demagnetization above 25–30 mT. The sediments below the Thimi geomorphic surface show dominantly normal polarity except for a short reverse polarity event near the base probably attributable to the Laschamp event (39–45 Ka). In the northwestern part, a prominent reverse polarity magnetozone occurs within the lower parts of the sections that are exposed below the Gokarna geomorphic surfaces. This implies to the deposition of the sediments yielding the reverse polarity prior to the Brunhes Normal Polarity Chron (i.e. before 780,000 yrs). This new discovery requires a thorough chronological study of the northern part of the valley with regard to the extent and distribution of such old deposits, which may directly correlate to the Lokundol Formation occurring widely in the southern part of the Kathmandu Valley.

INTRODUCTION

A number of investigations made on the Kathmandu Valley sediments in the eighties (Yoshida and Igarashi 1984; Dongol 1985; Igarashi et al. 1988; Yoshida and Gautam 1988) indicated their fluvio-lacustrine origin and a broadly Pliocene-Pleistocene chronological framework. Table 1 gives the existing stratigraphic scheme suggested from surface mapping and magnetic polarity stratigraphy on limited sections. The radiocarbon ages reported so far are widely variable. According to Yoshida and Igarashi (1984), the younger-stage deposits are dated between 30 and 10 Ka. Igarashi et al. (1988) noted a radiometric date of 45,300 yrs B.P. for the Thimi Formation but attributed it to the age of the possibly redeposited wood fragment, possibly derived from older formations. More recently, Gajurel (1998) obtained radiocarbon dates of 45,140±1,160 yrs B.P. and 43,180±1,310 yrs B.P. for two samples situated ca. 12 m apart along the vertical within the section, believed to belong to Thimi Formation, exposed at the quarry at Thimi and interpreted them as depositional ages. If true, the lower limit of the Thimi Formation extends back to ca. 45,000 yrs B.P.. The sedimentation rate of 5.9 mm/yr implied by these ages, however, may be rather high for the fluvio-lacustrine environment. It is notable that these sediments have provoked renewed interest for geological (biostratigraphic, sedimentological and structural), geomorphological, seismotectonic and geochronological studies (Pandey 1992; Saijo et al. 1995; Gajurel et al. 1998; Sakai and Tabata 2001; Sakai et al. 2001) partly because of their vast potential towards understanding many interrelated phenomena such as Himalayan uplift, monsoon climate, etc. (Fujii and Sakai 2002; Sakai et al. 2002).

In this paper, we briefly describe new magnetic polarity scheme of the sediments that are exposed in the sections extending below the Thimi and Gokarna geomorphic surfaces. Besides polarity data, magnetomineralogy essential for understanding the magnetic remanence carriers is briefly described. This study was aimed at establishing a refined and more detailed chronostratigraphic framework for these deposits through denser sampling especially in the central and northern part of the Kathmandu Valley.

GEOLOGICAL CROSS-SECTIONS AND SAMPLING

The samples for magnetostratigraphic study were taken from silt/clay and fine sand layers (lacustrine beds) from sections within the central and northwestern parts of the Kathmandu Valley. Depending on the stratigraphic position of the tops of these sections, they are fully or partly thought to be representative of Thimi Formation and Gokarna Formation as shown under sector c and sector d, respectively (Fig. 1). The spacing of sampling levels is widely variable as it was dictated by the availability of suitable layers along the sampled sections.

Table 1: Stratigraphic framework of the Kathmandu Valley sediments (modified after Yoshida and Igarashi 1984).

Division	Formation (Fm.)	Age** range determined by radiocarbon (^{14}C) method (yr. BP) and magnetostratigraphy		Distribution
Younger-stage deposits (lacustrine and deltaic in origin)	Patan Fm.	**(1)** 11,000-19,000 (11,070±290 to 18,970±1,480)		Central and northern parts of the valley. The topmost parts are marked by distinct terrace surfaces (younging towards the valley center).
	Thimi Fm.	**(2)** 24,000-28,000 (>23,390 to 33,200)	**(4)** $45,300 \pm^{6,100}_{3,400}$	
	Gokarna Fm.	**(3)** 28,000-30,000 (24,420±1990 to $29,390 \pm^{2,660}_{2,040}$)	**(5)** 43,180±1,310 **(6)** 45,140±1.160	
Middle-stage deposits (terrace/fan gravel)	Pyanggaon Fm. Chapagaon Fm. Boregaon Fm	Possibly middle Pleistocene		Southern part of the valley.
Older-stage deposits (lacustrine origin)	Lukundol Fm.	**(7)** Late Pliocene- early Middle Pleistocene (Gauss Chron to early (?) Brunhes Chron)		Widespread in the south. Probable subsurface occurrence in the north.

** (1)-(3): most probable age range (followed by a broader range based on compilation by Yamanaka and Yoshida) afterYoshida and Igarashi (1984). These ranges incorporate data obtained by Yonechi (1973); (4): after Igarashi et al. (1988); (5) & (6): Gajurel (1998); and, (7): Yoshida and Gautam 1988).

A NNE-SSW profile depicting the lithologs, of well-exposed vertical sections lying below the Thimi geomorphic surface (in area c, Fig. 1), is described by Sakai T. et al. (2001). Except for a small part in the south belonging to the Patan Formation, the upper parts of these sections belong to the Thimi Formation. The lower parts of some of them may belong to the Gokarna Formation but there are no data that allow definitive assignments. Judging from the depositional environment, four distinct facies are recognized: delta plain, delta front, prodelta and alluvial fan deposits. Four sections or their parts (API, APG, SA-SB and APB) were subjected to magnetostratigraphic study as shown later in Fig. 5. The sampled part of API (i.e. above about 1,318 m) and the whole APG section comprise sediments that are interpreted as deposits of successive (at least 3 in the former, and 4-5 in the latter) fluvial channel/delta plain aggradation cycles (Sakai T. et al. 2001). Similarly, the lower un-sampled part of API and the sampled part of APB belong to the delta-front deposits, formed after the lake level rise that induced the delta plain aggradation forming the SA-SB sections, believed to be much older in age.

The lithological correlations and sedimentological/ depositional characteristics of the sections below the Gokarna geomorphic surfaces (in area d, Fig. 1) have been described by Sakai and Tabata (2001). Only the southernmost and northernmost ends are characterized by exposures of the Thimi Formation and bedrock, respectively. In general, the facies are predominated by delta plain (channel, marsh, interdistributary bay etc.) deposits. Delta front and prodelta deposits occur intermittently with the delta plain deposits whereas alluvial fan and alluvial cone deposits are localized in the lower parts of the sections in the north. Accessible parts from four sections (LUB, GOC-LUA, GOF and GOM) were subjected to magnetostratigraphic study as shown later in Fig. 6. The GOM section is represented mainly by prodelta and delta front deposits and contains diatomite-bearing layers. Sampled part of GOF section is represented by delta plain, channel-marsh-interdistributary bay etc. and, to some extent, also by prodelta deposits. Sakai and Tabata (2001) suggested the presence of an erosion surface at the basal part of the LUB section and correlated it with the surface passing in between the alluvial fan and alluvial cone deposits in the sections lying to the south (e.g. GOC-LUA). According to this interpretation, the alluvial fan deposits are truncated by alluvial cone deposits, which in turn, are overlain by delta plain deposits as onlaps on the top of the alluvial cone.

Four to eight oriented specimens were obtained from each sampled level/site by inserting nonmagnetic polyethylene cubic boxes (7 cc or 10 cc) directly into the outcrop formed by the semi-consolidated sediments by shaping into a near-vertical shape. A fiducial mark drawn on each plastic box recorded the strike azimuth and sense of dip of each sampled face. Each box was sealed with a cap so as to retain the moisture.

LABORATORY PROCEDURE

In the laboratory, a set of selected cubic specimens was subjected to stepwise alternating field demagnetization (AFD) using fields between 0 and 100 mT with 5 mT steps. Remanence measurements were performed using a RF SQUID magnetometer (2G Enterprises, with noise level <0.01 mA m^{-1}. A series of static tri-axial demagnetizers capable of generating up to 150 mT peak fields was attached to the magnetometer. As pilot demagnetization data showed an erratic demagnetization response above ca. 65 mT, the remaining specimens were treated using AFD up to 65 mT.

The variation of low-field magnetic susceptibility (k) with temperature was recorded for small volumes of specimens (ca. 0.25 cm^3) using a Kappabridge system (AGICO KLY-3 with an attached CS-3 furnace). The heating-cooling cycle

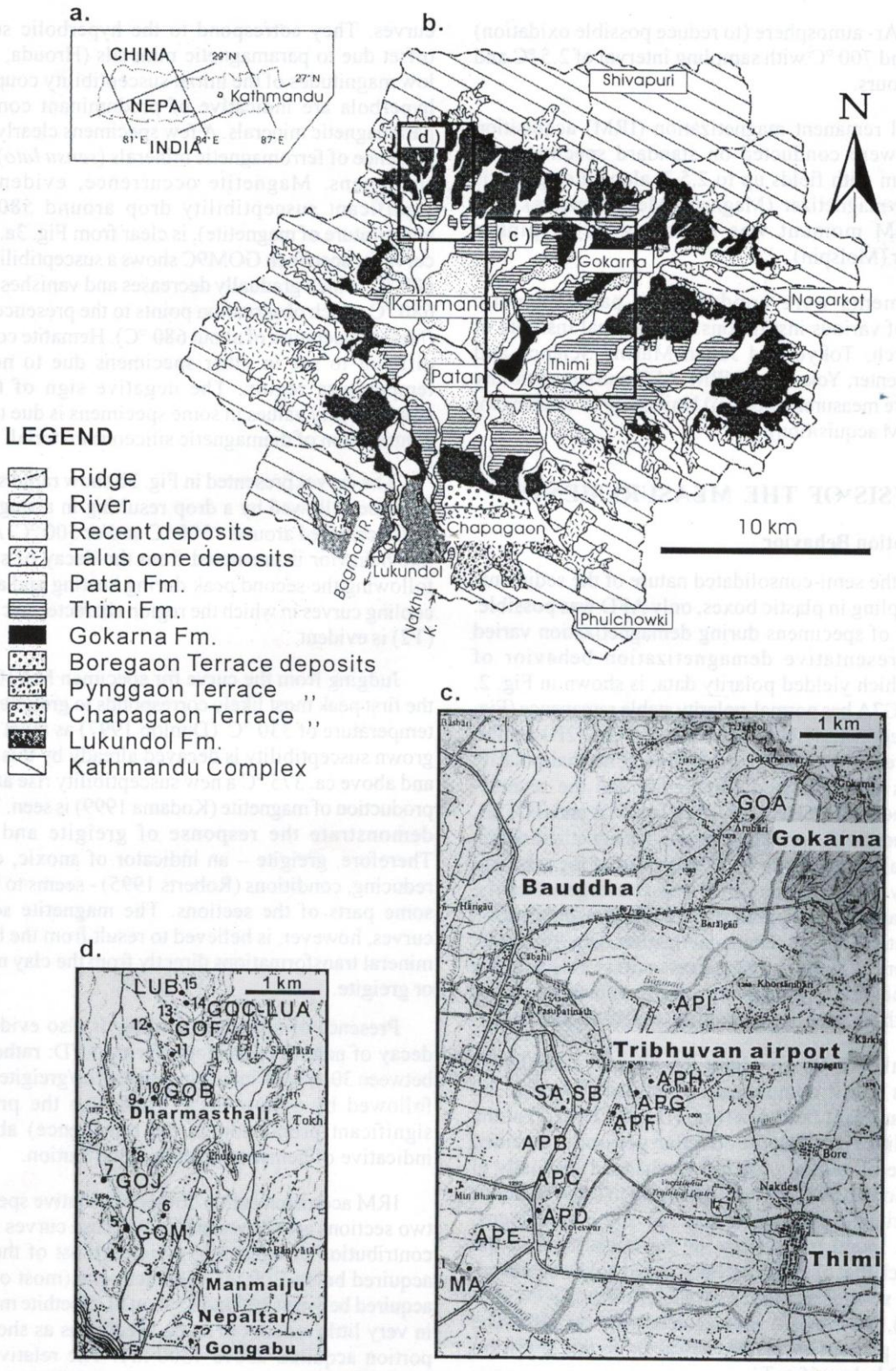

Fig. 1: Sketch maps showing the general geological divisions of the Kathmandu Valley and the localities studied. a) Index map; b) Geological divisions (after Yoshida and Gautam 1988); c) Localities mainly represented by Thimi Formation, sampled at Manohara River (MA), around the airport (APB-API), at Sinamangal (SA, SB) and at Arubari near Gokarna (GOA); and d) Localities represented by mainly Gokarna Formation (GOB-GOM) and older deposits tentatively equated to the Lukundol Formation (LUA, LUB) during the sampling stage.

took place in Ar- atmosphere (to reduce possible oxidation) between 40 and 700 °C with sampling interval of 2.5 °C and lasted for 2-hours.

Isothermal remanent magnetization (IRM) acquisition experiments were conducted on standard specimens by imparting them with fields up to 2.5 T along a single-axis using a pulse magnetizer (Magnetic Measurements). The acquired IRM moment was measured by a spinner magnetometer (Molspin).

Measurements were conducted at paleomagnetic laboratories of various institutions: (i) National Institute of Polar Research, Tokyo and Japan Marine Science and Technology Center, Yokosuka (NRM, AFD and susceptibility vs. temperature measurements), (ii) University of Tuebingen, Germany (IRM acquisition).

ANALYSIS OF THE MEASUREMENTS

Demagnetization Behavior

Owing to the semi-consolidated nature of the sediments and their sampling in plastic boxes, only AFD was possible. The behavior of specimens during demagnetization varied widely. Representative demagnetization behavior of specimens, which yielded polarity data, is shown in Fig. 2. Specimen APG7A has normal-polarity stable remanence (Fig. 2a). Three specimens (LUA3A, SA1A and GOF2B) exhibit dual polarity remanence. In LUA3A, the soft normal-polarity component is demagnetized completely and the reverse-polarity remanence is isolated (Fig. 2b). In SA1A and GOF2B, a soft-component with normal polarity is demagnetized within applied AF values as shown by distribution of the resultant NRM roughly along a great-circle and convergence of the direction towards the antipodal region; the demagnetization is not complete (Fig. 2c). Demagnetization data from such specimens were analyzed by remagnetization circle analysis to extract the reverse-polarity stable remanence and combined with the stable end-points, whenever available.

In general, AF up to about 25-30 mT completely demagnetizes a soft component, which was found to be closer to the ambient field direction (D = 0°, I = 47°) at the sampled locality. After that the direction generally remained stable (in case of normal polarity) or changed gradually to antipodal region up to 60-65 mT. Above 65 mT, the behavior of most specimens became erratic. In some specimens, intensity was found to decrease to the noise level of the instrument such that a stable direction could not be achieved. In contrast, in several specimens, especially from GOM sites (Fig. 1 and 6), the intensity was reduced only by 60%. The characteristic primary directions extracted in this study are based on AFD below 65 mT.

Magnetomineralogy

Fig. 3 shows the magnetic susceptibility vs. temperature curves. Presence of gently sloping segments in the initial part, between 30 and 200-300 °C, is evident in all heating curves. They correspond to the hyperbolic susceptibility offset due to paramagnetic minerals (Hrouda, 1994). Very low magnitudes of the initial susceptibility coupled with the hyperbola are indicative of predominant contribution of paramagnetic minerals. A few specimens clearly indicate the presence of ferromagnetic minerals (*sensu lato*) in unheated specimens. Magnetite occurrence, evidenced by the significant susceptibility drop around 580 °C (Curie temperature of magnetite), is clear from Fig. 3a. The heating curve for specimen GOM9C shows a susceptibility tail, above 600 °C, which gradually decreases and vanishes around 675-680 °C. Such observation points to the presence of hematite (Neel temperature of about 680 °C). Hematite contribution is difficult to see in other specimens due to noise at high temperature region. The negative sign of the residual susceptibility values in some specimens is due to significant contribution of diamagnetic siliceous material.

The curves presented in Fig. 3b show rapid susceptibility increase followed by a drop resulting in a single or double peaks centered around <300 °C and/or 500 °C. A magnetite-like behavior is presumed from the decay of susceptibility following the second peak during heating and also from the cooling curves in which the region characteristic of magnetite (T2) is evident.

Judging from the curve for specimen MA10C (Fig. 3b), the first peak most likely corresponds to greigite with a Curie temperature of 330 °C (Dunlop 1997) as most of the newly grown susceptibility is decayed already by this temperature and above ca. 375 °C a new susceptibility rise attributable to production of magnetite (Kodama 1999) is seen. These curves demonstrate the response of greigite and magnetite. Therefore, greigite – an indicator of anoxic, e.g. sulphate reducing, conditions (Roberts 1995) - seems to be present in some parts of the sections. The magnetite seen in these curves, however, is believed to result from the heat-induced mineral transformations directly from the clay minerals and/or greigite.

Presence of mixed mineralogy is also evident from the decay of natural remanence during AFD: rather fast decay between 30–65 mT indicating magnetite/greigite contribution followed by a slow decay (and also the presence of a significant proportion of the remanence) above 65 mT indicative of hematite/goethite contribution.

IRM acquision curves for representative specimens from two sections are shown in Fig. 4. These curves clearly show contribution of magnetite/greigite (most of the remanence acquired below 300 mT) and hematite (most of the portion acquired between 300 and 1500 mT). Goethite may be present in very little amount in some specimens as shown by some portion acquired above 1500 mT. The relative content of magnetic minerals in samples from GOM sites is clearly several times higher than those from API.

Among the very fine sediments, relatively low susceptibilities were found for GOM specimens, possibly caused by higher concentrations of diamagnetic SiO_2, than

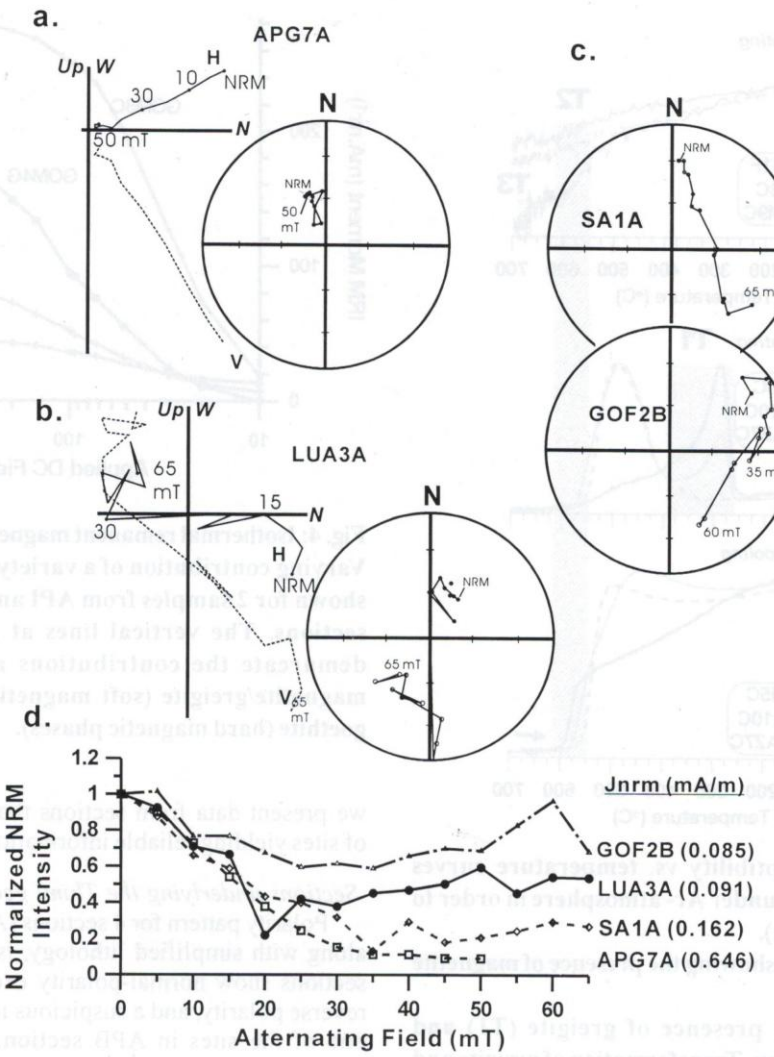

Fig. 2: Demagnetization behaviour of representative specimens yielding polarity information. Orthogonal vector plots and equal-area projections of the vector end-points for two specimens exhibiting only normal (APG7A) and dual-polarity (LUA3A) are shown in (a) and (b), respectively. In (c), results for two specimens (SA1A and GOF2B) that exhibit dual-polarity nature reflected in the roughly great-circle distribution of the resultant NRM directions after successive AFD cleaning steps are shown. The directions are shown in geographical coordinates. (d) Normalized intensity response curves for all representative specimens.

in specimens from other sections. The single-domain nature of magnetite is suggested by elevated ARM magnitudes. In particular, differences in magnetic mineralogy (amount, size, type) were found between parts that lie below and above the GOM7 level. The samples comprising GOM section possess the highest stability and consistency, especially above GOM 7 (diatomite-bearing layers). Both magnetite and hematite contribute to the natural remanence.

Estimation of Characteristic Remanence and Criteria for Polarity Determination

Analysis and calculation of the characteristic remanence defined by or remaining after 15-65 mT were carried out using the Munich University program called PALMAG incorporating principal component analysis (Kirschvink 1980). Directions were commonly estimated by fitting a line to a series of data points obtained after successive demagnetization steps (e.g. for APG7A and LUA3A shown in Fig. 2a; for ranges see Table 2) anchoring to the origin. When an obvious stable direction was not achieved but there were clear indications of convergence to reverse-polarity direction shown by a series of data points lying along a great-circle trend in a stereoplot, remagnetization circle analysis offered by PALMAG was performed. Mean directions at site level were estimated by combining specimen directions and/or remagnetization circles with maximum angular deviation (MAD) smaller than 20° (Table 2). Though the a_{95} angle is quite large for some sites, the mean directions

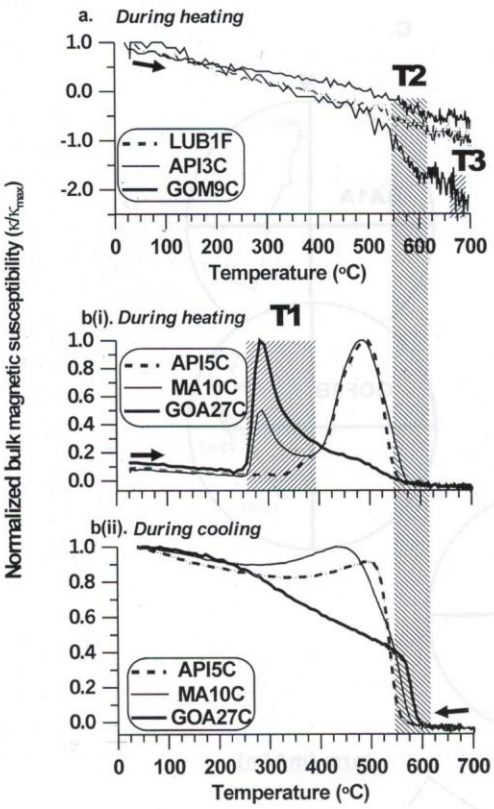

Fig. 3: Magnetic susceptibility vs. temperature curves (experiments conducted under Ar- atmosphere in order to reduce possible oxidation).
a. Response of specimens showing the presence of magnetite (T2) and hematite (T3).
b. Curves showing the presence of greigite (T1) and paramagnetic contribution. Transformation of greigite and clay minerals to magnetite is inferred from joint analysis of the heating and cooling curves. For clarity, the heating and cooling curves are shown separately and at differing vertical scales. Note that the susceptibility in each curve is normalized to the maximum value.

are thought to be fairly usable for the polarity determination but the use of these directions for analyzing small-scale variations (e.g. secular variations) is not recommended. Polarity determination is based on the values of virtual geomagnetic pole latitude (Normal: >30°; Reverse: <30°; Indeterminate: -30° to +30°) calculated using the mean direction at each site.

Magnetic Polarity Stratigraphy

Samples from all sections shown in Fig. 1 were subjected to alternating field demagnetization. For several sections, a large proportion of the specimens showed very weak NRM intensities and had to be rejected from further analysis. This resulted in either drastic reduction in the number of usable samples and/or very uneven distribution along the thickness column. The polarity information obtained from such sections seemed not to be adequate. In the following section,

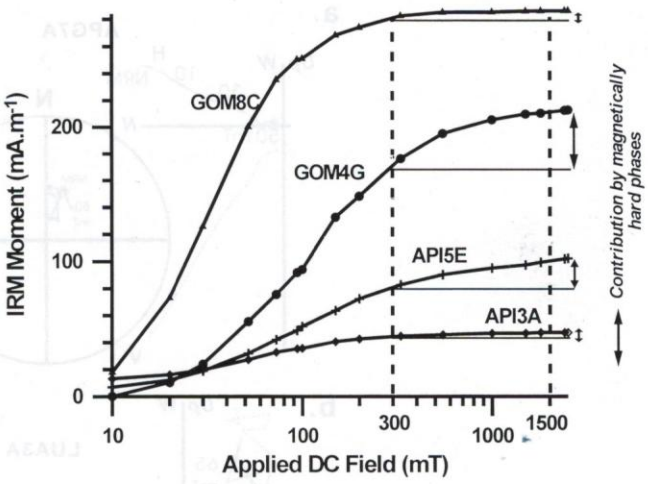

Fig. 4: Isothermal remanent magnetization acquition curves. Varying contribution of a variety of magnetic minerals is shown for 2 samples from API and 2 samples from GOM sections. The vertical lines at 300 mT and 1500 mT demarcate the contributions attributable mostly to magnetite/greigite (soft magnetic phase) and hematite/ goethite (hard magnetic phases).

we present data from sections that have adequate number of sites yielding reliable information.

Sections underlying the Thimi geomorphic surface

Polarity pattern for 4 sections (API, APG, SA-SB, APB), along with simplified lithology, is shown in Fig. 5. These sections show normal-polarity except for site SA1 with a reverse polarity, and a suspicious indeterminate polarity for one of the sites in APB section. A tentative composite polarity diagram is shown in the right side of Fig. 5. The portion shown in light gray shade represents an inferred normal polarity. Considering the available radiocarbon ages and also the reverse polarity event closest to them, the reverse polarity is attributed to the Laschamp Subchron, whose dates are constrained within 39-45 kyr range with a mean of ca. 42 kyr (Champion et al. 1988).

Sections underlying the Gokarna geomorphic surfaces

Fig. 6 shows 4 sections (LUB, GOC-LUA, GOF and GOM) with simplified lithology and polarity interpretation. There is a prominent reverse polarity magnetozone at the base of the GOC-LUA and GOF sections. The reverse polarity zone at the middle of GOF section is supported by just one site and so its extent is poorly constrained. The GOM section has exclusively normal polarity.

INTERPRETATION AND DISCUSSION

Sections underlying the Thimi geomorphic surface

The occurrence of the reverse polarity event, correlatable to Laschamp Subchron, is in accord with the ^{14}C dates of 45 kyr and 43 kyr obtained by Gajurel (1998) for two levels lying

Table 2: Mean characteristic remanence directions (in stratigraphic coordinates) and derived polarity. GC stands for great circle analysis method. Indeterminate polarity is shown by a question mark.

Site	AFD Range (mT)	n	Decl.(°)	Incl.(°)	k	a_{95}(°)	VGP latitude (°)	Polarity
GOM1	15-50	6	353.8	34	10.8	21.4	79.3	Normal
GOM2	15-50	6	9.6	30.6	17.3	15	75.7	Normal
GOM3	20-50	7	6.1	26.4	14.2	16.6	75.1	Normal
GOM4	25-60	7	16.3	45.6	20.6	13.6	75.5	Normal
GOM5	20-80	7	354.3	36.3	32.4	10.8	80.8	Normal
GOM6	20-60	5	329.9	42.7	27.3	14.9	62.9	Normal
GOM7	15-65	7	351.6	33.2	76.6	6.9	77.7	Normal
GOM8	10-55	7	350	45.4	208.3	4.2	81.1	Normal
GOM9	5-65	7	348.5	50.2	250.4	3.8	79.5	Normal
GOM10	15-50	6	330.9	42.5	66.2	8.3	63.8	Normal
GOF1(i)	25-55	3	311.5	18.5	19.2	28.9	40.9	Normal
GOF1(ii)	10-60	3	222.5	-29.4	2157.6	14.3	-49.0	*Reverse*
GOF2	0-65	5	200.3	-42	15.3	29.2	-71.4	*Reverse*
GOF3	0-60	6	202.1	-32.9	22.1	18.7	-67.5	*Reverse*
GOF4(i)	30-60	2	11	24.5			71.9	Normal
GOF4(ii)	5-60	4	215.2	-47.7	44.9	26.7	-59.1	*Reverse*
GOF5	10-60	4	191.5	-38.8	49.5	25.4	-78.1	*Reverse*
GOF6	30-65	4	301	20.6	41.1	51.9	32.3	Normal
GOF7	0-65	4	144.1	-15.9	96.4	18.1	-50.9	*Reverse*
GOF8	10-65	5	347.4	34.4	38.3	12.5	75.5	Normal
GOF9	20-65	5	358.4	24.7	80.8	8.6	75.2	Normal
LUA1	20-65	5	196.9	-32.9	36.5	18.7	-71.6	*Reverse*
LUA2	20-65	4	192.8	-38.5	673	6.8	-76.9	*Reverse*
LUA3	20-65	4	191.2	-36.5	45	26.6	-77.4	*Reverse*
GOC1	mainly RC	7	171.3	7.3	48	12.7	-57.5	*Reverse*
GOC2	mainly RC	4	203.2	-55.1	19.1	41.5	-68.8	*Reverse*
GOC3	mainly RC	3	187.3	24.8	398.7	10.5	-48.7	*Reverse*
GOC4	mainly RC	5	179	-42.5	41	17.6	-86.8	*Reverse*
LUB1	20-65	6	23.1	40	99.4	6.8	68.6	Normal
LUB2	20-65	6	241.5	18.1	14.6	18.2	-20.0	*?*
LUB3	20-65	6	35.4	25.1	20.1	15.6	54.0	Normal
LUB4	20-65	6	359	29.8	142.8	5.6	78.2	Normal
LUB5	20-65	6	365.15	22.35	103.15	10	70.9	Normal
API1	20-65	5	345.2	24.8	109.3	7.4	69.8	Normal
API2	25-55	5	2.7	36.5	68.3	9.3	82.2	Normal
API3	10-50	2	291.5	7.4			20.7	*?*
API4	15-60	5	8.6	27.5	37.3	12.7	74.6	Normal
API5	30-50	5	357.3	30.3	12.9	22.1	78.3	Normal
API6	25-65	5	6	20.1	12.3	22.7	71.8	Normal
API7	0-50	3	286.7	67	16.6	31.3	31.3	Normal
APG1	10-30	1	1.7	20.4			72.8	Normal
APG2	40-65	5	19.1	34.2	56.4	10.3	70.3	Normal
APG3	15-50	4	5.1	33.7	26.8	18.1	79.6	Normal

Contd.....

Table 1 (continued)

APG4		4	very low intensity				-	
APG5	15-65	5	338.5	50.1	6.7	32	71.0	**Normal**
APG6	15-60	5	359.6	46.7	5.6	35.6	89.6	**Normal**
APG7	30-50	5	12.8	52.7	36.2	12.9	77.7	**Normal**
APG8	10-50	4	335.6	32.4	17	30.3	65.4	**Normal**
APG9	25-50	4	341.5	30	138.9	8.3	69.3	**Normal**
APG10	15-65	5	347.9	40.3	45.9	11.4	78.1	**Normal**
SA1	0-65	4	181.3	-39.4	55	24	-84.5	*Reverse*
SA2	50-65	4	358.8	31.2	386.4	4.7	79.1	**Normal**
SB1	45-65	4	352.6	36.8	220.3	6.2	80.1	**Normal**
SB2	50-65	4	306.8	22.3	149.1	7.5	37.8	**Normal**
APB1	35-60	4	8.8	43	8	34	81.7	**Normal**
APB2	30-55	5	23.8	44.8	54	10.5	68.8	**Normal**
APB3	35-65	5	29.8	36.5	10	25.4	61.9	**Normal**
APB4	20-50	3	49.5	31.5	8	46.8	43.3	**Normal**
APB5	30-60	5	21.4	31.8	115.7	7.1	67.7	**Normal**
APB6	40-65	4	24.2	29.1	25.8	18.4	64.5	**Normal**
APB7	25-65	5	22.5	42.1	13.8	21.3	69.5	**Normal**
APB8	25-50	5	1.9	55.6	41.1	12.1	81.4	**Normal**
APB9	30-50	5	24.5	33.6	95.6	7.9	65.7	**Normal**
APB10	25-50	5	20.4	27.5	53.7	10.5	67.0	**Normal**
APB11	25-50	3	38.3	16.5	14.7	33.3	49.1	**Normal**
APB12	30-60	5	40.1	16.6	15.9	19.8	47.6	**Normal**
APB13	25-55	5	36.1	31.9	18.2	18.4	55.2	**Normal**
APB14	35-65	5	29.7	29	49.3	11	59.9	**Normal**
APB15	40-60	5	30.1	25.7	7.9	29	58.6	**Normal**
APB16	40-65	5	48.7	23.1	67.1	9.4	41.9	**Normal**
APB17	20-65	5	45.7	31	42.3	11.9	46.5	**Normal**
APB18	40-50	4	91.8	10	7.7	35.4	0.8	*?*
APB19	40-65	5	29.7	39.8	36.7	12.8	62.7	**Normal**
APB20	35-65	5	20.8	34.5	55.3	10.4	69.0	**Normal**
APB21	30-65	5	7.7	33.6	37.4	12.7	78.3	**Normal**

Note: RC= great circle analysis; n = no. of samples used in calculation of the mean direction. Decl. = declination; Incl.= Inclination; k = precision parameter; a_{95} = cone of 95% confidence level; VGP = virtual geomagnetic pole

between 1300-1320 m altitude at Thimi quarry (Fig. 5). There are two possible scenarios to explain the relationship between the Thimi and Gokarna formations and the ages exceeding 40 kyr:

1. The lower parts of the sections underlying the Thimi geomorphic surface actually form the lower part of the Thimi Formation formed due to aggradation and subsequent progradation of delta deposits (refer to Sakai et al. 2001). This occurred during the temporary fall in lake level during the Gokarna accumulation phase within the inner parts of the basin characterized by the accumulation of the Gokarna Formation. In this case, the Gokarna Formation is unconformably overlain by Thimi Formation sediments that differ in age depending on the particular position within the depositional basin.
2. The lower parts of the sections underlying the Thimi geomorphic surface belong to the Gokarna Formation rather than the Thimi Formation. This is also plausible because aggradation of delta deposits is observed in the lower part of the Gokarna Formation (Sakai et al. 2001). In this case, the older ages (>40 kyr) can be easily attributed to the Gokarna Formation.

Preference to one of these scenarios requires further evidences through analysis of all available data on Thimi and Gokarna formations and probably also the acquisition of additional properties (e.g. rock-magnetic parameters) that may allow definitive lateral comparison of these sections.

Sections underlying the Gokarna geomorphic surface

It was noted earlier that the basal part of LUB and the lower part of GOC-LUA are comparable on lithological basis.

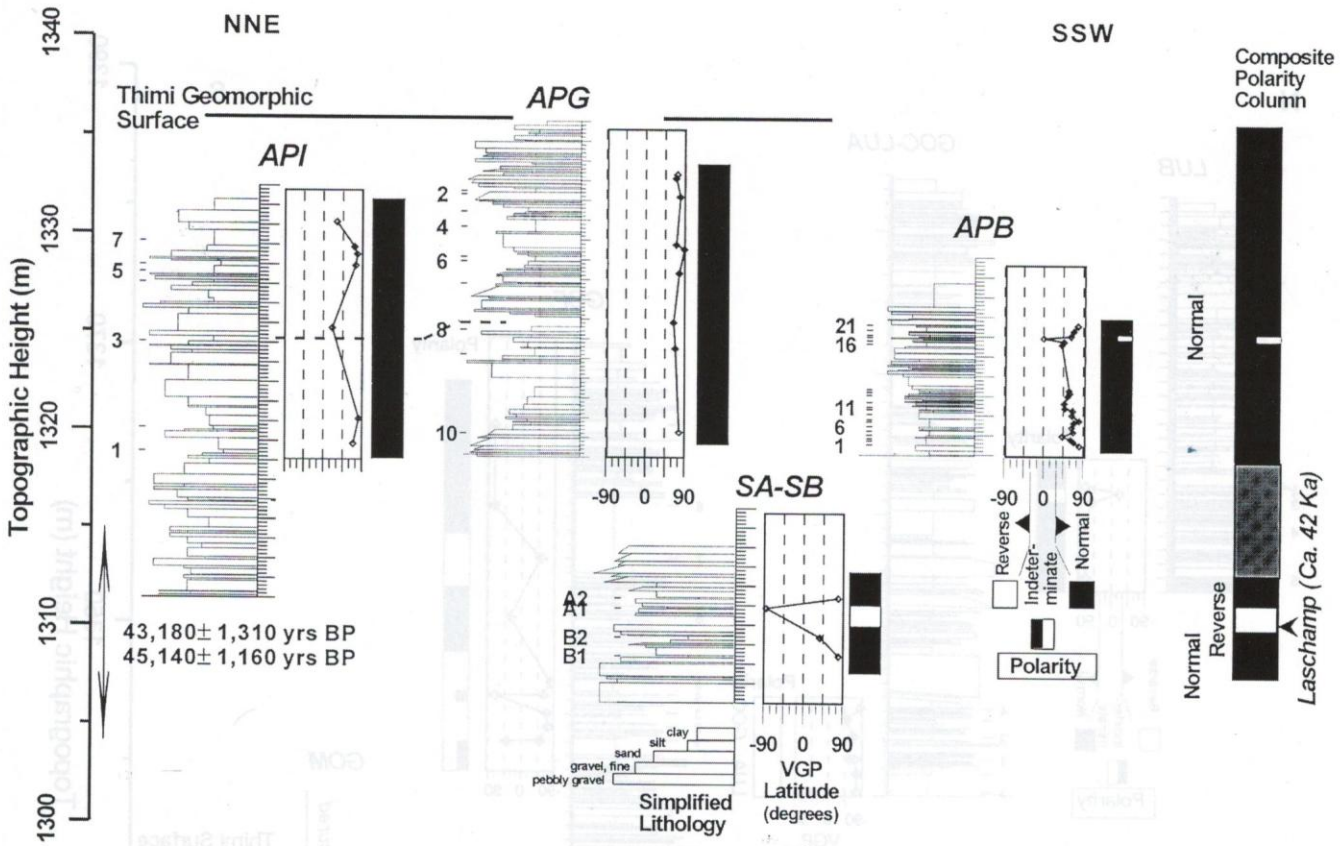

Fig. 5: Simplified lithologs, sampling levels and plots of the virtual geomagnetic pole (VGP) latitudes with the inferred magnetic polarity sequence (MPS) for the sections underlying the Thimi geomorphic surface. Radiocarbon (^{14}C) dates after Gajurel (1998) for the Thimi section (not shown here) are given against the altitude range for reference. For map positions of the sections refer to Fig. 1c.

However, the completely reverse-polarity of the lower part of GOC-LUA and the contrasting normal polarity at the base of LUB suggest that there is no synchroneity between these lithologically comparable segments. Then, the erosion surface in the lower part of LUB is likely to be of local nature. Likewise, the alluvial fan deposits also seem to be distributed locally.

The reverse polarity zones in sections GOC-LUA and lower part of GOF span for at least 6 m and 4 m, respectively (Fig. 6). The reverse polarity recorded by them represents a reversal of the geomagnetic field; it cannot be a self-reversal as the remanence is purely detrital one and the sediments have not experienced significant reheating ruling out any acquisition of partial thermoremanence.

In the absence of any independent age data from these lower levels of the sections, one may argue that this reverse magnetization was possibly acquired during one of the known polarity excursions/subchrons/events (such as Laschamp, Blake, Jamaica, Lavantine, Biwa III, Emperor, Big Lost and Delta excursions – which are regarded as significant by Champion et al. 1988) during the Brunhes Normal Polarity Chron. However, the duration of these excursions is believed to be $<10^4$ yrs (McElhinny and McFadden 2000), which means that a 4-6 m thick sediment column requires an accumulation rate of 0.4 to 0.6 mm/yr - that is almost an order of magnitude greater than the 0.07 mm/yr average rate suggested for the Lukundol Formation (Yoshida and Gautam 1988). Though this possibility can not be firmly denied, it is more reasonable to consider that these reverse-polarity intervals correspond to the Pre-Brunhes age (i.e. 0.78 Ma), the most likely candidate being the earlier part of the Matuyama Reverse Polarity Chron (0.780–2.581 Ma). The GOM section with exclusively normal polarity can't be definitively correlated to the sections lying to the north without further analyzing additional characteristics.

From the above reasoning, the reverse polarity segments recorded in the GOC-LUA and GOF sections (Fig. 6) correspond to the younger part of the magnetozone K2 recorded within the Lukundol Formation in the southern part of the Kathmandu Valley. A more definite age range of these sections and a better comparison with the Lukundol Formation, in terms of lithology, sedimentological characteristics etc. requires further analysis, and determination of rock-magnetic parameters on densely sampled sections in both areas may be helpful.

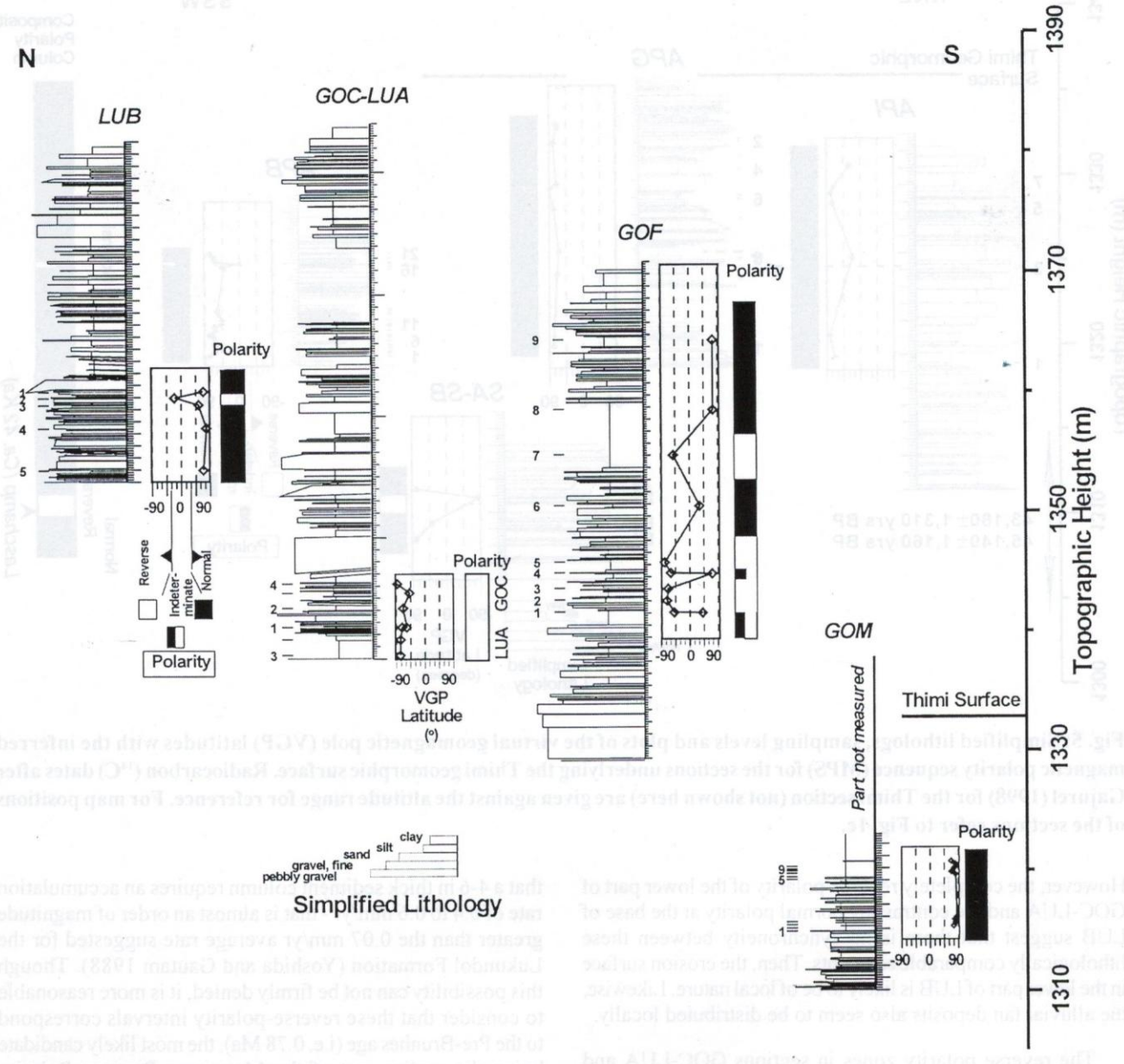

Fig. 6: Simplified lithologs, sampling levels and plots of VGP latitudes with the inferred MPS for the sections lying below the Gokarna geomorphic surfaces. The positions of the sections are shown in Fig. 1d.

CONCLUSIONS

Magnetostatigraphic data from several sections in the central and northwestern parts of the Kathmandu Valley lead to the following conclusions:

1) The sediments from the central part, which is represented by the Thimi Formation, possess a dominantly normal polarity record. A confirmed reversal at the lower part of the sections underlying the Thimi geomorphic surface is tentatively related to the Laschamp event (39–45 kyr). If this is true, the lower age of the Thimi Formation extends well below 40 kyr implying that the older ages obtained recently (e.g. Gajurel 1998) are reasonable. Alternatively, these lower parts belong to Gokarna Formation.

2) The basal parts of the sections from the northwestern part, underlying the Gokarna geomorphic surfaces, are characterized by significant reverse polarity magnetozone. This magnetozone is related to the Matuyama Reverse Polarity Chron or even older times. Hence, the sedimentary sequences exposed at the lower parts of some sections in the northwestern part of the Kathmandu Valley are much

older than the ages assigned for the younger-stage deposits.

3) The presence of older sediments (pre-dating 780,000 yrs.) in the northern part of the Kathmandu Valley requires a revision of the existing models of sediment deposition and chronological reconstructions. Interpretation of the polarity data in terms of age may require revision once more accurate data on age, magnetic proxy parameters, sedimentological comparison, being currently investigated by various groups, will be available.

ACKNOWLEDGEMENTS

This paper originates from the M. Sc. Dissertation of AH at Hokkaido University. AH very much appreciates the advices and suggestions from Y. Fujiwara during laboratory studies and from H. Tabata during the fieldwork. Similarly, for access to the facilities at the paleomagnetic laboratories and invaluable guidance during measurements, she is grateful to M. Funaki (National Institute of Polar Research) and T. Kanamatsu (Japan Marine Science and Technology Center). PG thanks E. Appel for access to the laboratory at the University of Tuebingen.

This manuscript benefited from the critical comments of C. Crouzet, H. Sakai and an anonymous reviewer. Fieldwork in Nepal was done under research collaboration between Tribhuvan University and Hokkaido University. This study was supported by a Grant-in-Aid for Scientific Research (A) from Japan Society for the Promotion of Science to K. Arita (11691112).

REFERENCES

Champion, D. E., Lanphere, M. A., and Kuntz, M. A., 1988, Evidence for a new geomagnetic reversal from lava flows in Idaho: Discussion of short polarity reversals in the Brunhes and late Matuyama polarity chrons. J. Geophys Res., 93, pp. 11667–11680.

Dongol, G. M. S., 1985, Geology of the Kathmandu fluviatile lacustrine sediments in the light of new vertebrate fossil occurrences. Jour. Nepal. Geol. Soc., v. 3, pp. 43–57.

Dunlop, D.J. and Ozdemir, O., 1997, Rock Magnetism: fundamentals and frontiers, Cambridge University press.

Fujii, R. and Sakai, H., 2002, Paleoclimatic changes during the last 2.5 myr recorded in the Kathmandu basin, central Nepal Himalayas. Jour. Asian Earth Sci., v. 20, pp. 255–266.

Gajurel, A. P., 1998, Geochemie isotopique et deformations synsedimentaires des depots du bassin de Kathmandou, Memoire de DEA de l'Universite de Grenoble, 30 p. (*in French*).

Gajurel, A. P., Huyghe, P., France-lanord, C., Mugnier, J. L., Upreti, B. N., and Le Fort, P., 1998, Seismites in the Kathmandu basin, Nepal. Jour. Nepal Geol. Soc., v. 18, pp. 125–134.

Hrouda, F., 1994, A technique for the measurement of thermal changes of magnetic susceptibility of weakly magnetic rocks by the CS-2 apparatus and KLY-2 Kappabridge, Geophys. Jour. Int., v. 118, pp. 604–612.

Igarashi, Y., Yoshida, M., and Tabata, H., 1988, History of vegetation and climate in the Kathmandu valley. Proc. Indian natn. Sci. Acad., 54A(4), pp. 550–563.

Kirschvink, J. L., 1980, The least-squares line and plane and the analysis of palaeomagnetic data. Geophys. J. R. astr. Soc., v. 62, pp. 699–718.

Kodama, K., 1999, *Paleomagnetism*. Tokyo University press, 248 p. (*in Japanese*).

McElhinny, M. W. and McFadden, P. L., 2000. *Paleomagnetism: Continents and Oceans*. Academic Press.

Pandey, M. R., Sikrikar, S. M., Chitrakar, G. R., and Pierre, J. Y., 1992, Ground classification (microzoning) of Kathmandu valley in the basis of microtremor survey. Bull. Dept. Geol., Tribhuvan Univ., Kathmandu, Nepal, v. 2(1), pp. 181–189.

Roberts, A. P., 1995, Magnetic Properties of sediments greigite (Fe_3S_4), Earth Planet. Sci. Lett.,134, pp. 227–236.

Saijo, K., Kimura, K., Dongol, G., Komatsubara, T., and Yagi, H., 1995, Active faults in southern Kathmandu basin, central Nepal. Jour. Nepal Geol. Soc., v. 11 (Sp. Issue), pp. 217–224.

Sakai, H., Fujii, R., and Kuwahara, Y., 2002, Changes in the depositional system of the paleo-Kathmandu lake caused by uplift of the Nepal Lesser Himalayas. Jour. Asian Earth Sci., v. 20, pp. 267–276.

Sakai, T., Gajurel, A. P., Tabata, H., and Upreti, B. N., 2001, Small-amplitude lake-level fluctuations recorded in aggrading delta deposits of the Upper Pleistocene Thimi and Gokarna formations, Kathmandu Valley, Nepal. Jour. Nepal Geol. Soc., v. 25 (Sp. Issue), pp. 43–51.

Sakai, T. and Tabata, H., 2001, Spatial facies change of the lacustrine delta deposits in the Gokarna Formation, Kathmandu Valley. Paleo-Kathmandu Lake, field excursion guide, pp. 22–42.

Yonechi, F., 1973, A preliminary report on the geomorphology of Kathmandu valley. Sci. Rep. Tohoku Univ. 7th Ser. (Geography), v. 23, pp. 153–161.

Yoshida, M. and Igarashi, Y., 1984. Neogene to Quaternary lacustrine sediments in the Kathmandu valley, Nepal. Jour. Nepal Geol. Soc., v. 4 (Sp. Issue), pp. 73–100.

Yoshida, M. and Gautam, P., 1988, Magnetostratigraphy of Plio-Pleistocene lacustrine deposits in the Kathmandu Valley, central Nepal. Proc. Indian natn. Sci. Acad., v. 54A(3), pp. 410–417.